




Activated carbons derived from sugarcane bagasse for high-capacitance electrical double layer capacitors

Authit Phakkhawan¹, Mati Horprathum², Narong Chanlek³, Hideki Nakajima³, Supinya Nijpanich³, Pisisit Kumnorkaew⁴, Samuk Pimanpang^{5,7,*}, Pawinee Klangtakai^{1,6,7,*} , and Vittaya Amornkitbamrung^{1,6,7}

¹Department of Physics, Faculty of Science, Khon Kaen University, Khon Kaen 40002, Thailand

²National Electronics and Computer Technology Center (NECTEC), National Science and Technology Development Agency (NSTDA), Pathum Thani 12120, Thailand

³Synchrotron Light Research Institute (Public Organization), 111 University Avenue, Muang District, Nakhon Ratchasima 30000, Thailand

⁴National Nanotechnology Center (NANOTEC), National Science and Technology Development Agency (NSTDA), Pathum Thani 12120, Thailand

⁵Department of Physics, Faculty of Science, Srinakharinwirot University, Bangkok 10110, Thailand

⁶Institute of Nanomaterials Research and Innovation for Energy (IN-RIE), NANOTEC-KKU RNN on Nanomaterials Research and Innovation for Energy, Khon Kaen University, Khon Kaen 40002, Thailand

⁷Thailand Center of Excellence in Physics (TheP), Chiang Mai University, P.O. Box 70, Chiang Mai 50202, Thailand

Received: 7 August 2021

Accepted: 1 November 2021

Published online:

16 November 2021

© The Author(s), under exclusive licence to Springer Science+Business Media, LLC, part of Springer Nature 2021

ABSTRACT

Activated carbon (AC) from sugarcane bagasse was prepared using a simple two-step method of carbonization and chemical activation with four different activating agents (HNO₃, H₂SO₄, NaOH, and KOH). Amorphous carbon structure as identified by X-ray diffraction was observed in all samples. Scanning electron microscopy revealed that the AC had more porosity than the non-activated carbon (non-AC). Specific capacitance of the non-AC electrode was 32.58 F g⁻¹ at the current density of 0.5 A g⁻¹, whereas the AC supercapacitor provided superior specific capacitances of 50.25, 69.59, 109.99, and 138.61 F g⁻¹ for the HNO₃ (AC-HNO₃), H₂SO₄ (AC-H₂SO₄), NaOH (AC-NaOH), and KOH (AC-KOH) activated carbon electrodes, respectively. The AC-KOH electrode delivered the highest specific capacitance (about 4 times of the non-AC electrode) because of its good surface wettability, the largest specific surface area (1058.53 m² g⁻¹), and the highest total specific pore volume (0.474 cm³ g⁻¹). The AC-KOH electrode also had a great capacitance retention of almost 100% after 1000 GCD cycles. These results demonstrate that our AC developed from sugarcane bagasse has a strong potential to be used as high stability supercapacitor electrode material.

Address correspondence to E-mail: samuk@g.swu.ac.th; pawinee@kku.ac.th

1 Introduction

Solar or wind powers are alternative energy resources that attract great research interest because they can address pressing environmental issues and the shortage of fossil fuels [1–4]. To provide continuous power, the green energy produced from these alternative resources need to be stored in energy storage devices which include regenerative fuel cell systems, electrochemical capacitors, and batteries [3–5]. Among these storage devices, an electrochemical capacitor, also known as supercapacitor or ultracapacitor, has emerged as a promising candidate because of its excellent power density, rapid charging–discharging rate, and great cycling stability [6–10]. Regarding charge storage mechanisms, there are two types of the supercapacitor: (1) an electrical double layer capacitor (EDLC) and (2) a pseudocapacitor (PDC). Charge storage of the first type involves separating electrostatic charges at the interface between an electrode and an electrolyte [5, 11, 12] without a chemical reaction. As a result, the EDLC enjoys fast charge–discharge rate and long cycling stability. The second type relies on the combination process of the first mechanism and an electrochemical reversible redox reaction [5, 11, 12]. The combination of the two processes commonly results in larger capacitance but lower cycling stability in comparison to those of the EDLC [13].

For the EDLC, carbon materials such as graphene [14], carbon nanotube (CNT) [15, 16], and activated carbon (AC) [4, 10, 17] have been utilized owing to their high electrical conductivity and excellent specific surface area [1, 9, 10]. Among these carbon-based materials, AC is a preferred choice owing to its readily available abundance, inexpensiveness, and environmental friendliness. There are two methods to synthesize AC, namely physical or thermal activation, and chemical activation [1, 8]. In the former, oxidizing gases, carbon dioxide (CO₂) or steam (H₂O) are used as activating agents, and high temperatures of about 850–1000 °C are employed to modify carbon [1, 8, 18–20]. In the latter, chemical agents are used alongside lower temperature in modifying the carbon structure [1, 8]. Different chemical agents produce different specific surface areas, pore sizes, and surface functional groups.

Biomass or biowaste, such as rice straw [9, 10, 21], rice husk [22], banana fibers [23], onion [24], orange

peel [3], reed straw [17], bamboo [4, 6], coconut shells [25], and sugarcane bagasse [26], has been modified into activated carbon that has found various applications. For example, Van et al. [27] prepared AC from rice husk by activating it with NaOH for preparing a supercapacitor electrode material. At the current density of 1 A g⁻¹, a specific capacitance of 198.4 F g⁻¹ was obtained. Subramanian et al. [28] used AC derived from banana fibers that were subjected to activating with ZnCl₂ as a supercapacitor electrode and received a good specific capacitance of 75 F g⁻¹ at the current density of 0.5 A g⁻¹, a value many times higher than that obtained from the non-activated one (1 F g⁻¹). Zhang et al. [6] demonstrated that AC derived from bamboo using KOH as an agent could achieve an excellent specific capacitance of 293 F g⁻¹ at the current density of 0.5 A g⁻¹, more than three times as large as that of the non-activated carbon (97.5 F g⁻¹). Doloksaribu et al. [29] synthesized AC from coconut shell by modifying it with KOH. The AC from coconut shell produced a specific capacitance of 110 F g⁻¹ [29]. To date, there have been no reports on the use of sugarcane bagasse, huge amounts of which are discarded every year in our local northeastern region of Thailand, as an active material in the EDLC applications. To add value to sugarcane bagasse, we harnessed its potential as a carbon source turning it into activated porous carbon in supercapacitor.

In this paper, activated porous carbon derived from sugarcane bagasse was synthesized using a simple two-step method of carbonization and chemical activation. Four different agents, acidic agents (HNO₃ or H₂SO₄) and basic agents (NaOH or KOH), were used for activating these carbon materials. Physical properties of the non-activated carbon (non-AC) and activated carbons (ACs) were thoroughly characterized to understand the effect of the activating agents. Furthermore, structural and chemical characteristics of the differently treated carbons were thoroughly studied to explain the electrochemical behaviors of the non-AC and AC electrodes.

2 Experimental

2.1 Synthesis of non-AC and AC

In the carbonization process, sugarcane bagasse (*Saccharum officinarum*) was dried under the sun for

6 days. The dried sugarcane bagasse was shaped into small pieces (about $0.5 \times 1 \times 1.5 \text{ cm}^3$) and then washed with deionized (DI) water under sonication for 30 min to remove impurities. The cleaned sugarcane pieces were dried at $100 \text{ }^\circ\text{C}$ ($5 \text{ }^\circ\text{C min}^{-1}$) for 24 h in an oven under an ambient atmosphere. The dried pieces were then calcined at $500 \text{ }^\circ\text{C}$ ($10 \text{ }^\circ\text{C min}^{-1}$) for 1 h in a tubular furnace under an Ar environment. The carbonized material was further heated at $800 \text{ }^\circ\text{C}$ ($10 \text{ }^\circ\text{C min}^{-1}$) for 2 h in the tubular furnace under the Ar atmosphere. The product was washed with 3 M hydrochloric acid (HCl, RCI Labscan Ltd., 37%) to remove organic contamination, followed by washing with DI water until its pH was the same as that of the DI water. Because it was not subjected to the activation process, this carbon was referred to as the non-activated carbon (non-AC).

To activate the carbonized material, it was mixed with a different type of chemical agents: nitric acid (HNO_3 , AnaPURE, 65%), sulfuric acid (H_2SO_4 , RCI Labscan Ltd., 96%), sodium hydroxide, (NaOH, EMSURE, 99%) or potassium hydroxide, (KOH, RCI Labscan Ltd., 85%) in a weight ratio of 1:1, i.e., 1 g of the non-AC was mixed with 1 g of either HNO_3 , H_2SO_4 , NaOH, or KOH. Next, the non-AC and chemical agent were thoroughly mixed by grinding in a mortar. Then, the mixed product was heated at $800 \text{ }^\circ\text{C}$ ($10 \text{ }^\circ\text{C min}^{-1}$) for 2 h in the tubular furnace under the Ar atmosphere. The obtained powder was soaked in 50 mL of 3 M HCl under 30 min stirring. Then, the suspension was washed with DI water until its pH was the same as that of the DI water. Next, the precipitate was dried at $100 \text{ }^\circ\text{C}$ ($5 \text{ }^\circ\text{C min}^{-1}$) in an oven under an ambient atmosphere for 24 h. The activated carbons (ACs) were denoted as AC- HNO_3 , AC- H_2SO_4 , AC-NaOH, and AC-KOH to correspond to the respective HNO_3 , H_2SO_4 , NaOH, and KOH agents used.

2.2 Preparation of electrodes

The non-AC or the AC, carbon black (C, Alfa aesar, 99%), and polyvinylidene fluoride (PVDF, Sigma-Aldrich, $M_w = 534,000$ by GPC) were mixed in a weight ratio of 80:10:10 with 5000 μL of N-methyl-2-pyrrolidone (NMP, Sigma-Aldrich, 99%). The resulting homogeneous slurry was coated onto a Ni foam ($1 \times 1 \text{ cm}^2$). The coated electrode was then dried at $100 \text{ }^\circ\text{C}$ ($5 \text{ }^\circ\text{C min}^{-1}$) for 12 h in an oven under an ambient environment. A force of 10 kN (or a pressure

of 127.32 N cm^{-2}) was applied to the dried electrode, producing a thin, flexible film. The mass of active materials, determined by a semi-micro balance (Sartorius, Thailand), was approximately 2–4 mg.

2.3 Structural characterization

A desktop scanning electron microscope (MiniSEM, SEC, SNE-4500 M) attached with an energy dispersive X-ray (EDX) instrument was employed to characterize pore structures, morphologies, and elemental composition. Crystal structures of the non-AC and ACs were studied by X-ray diffraction (XRD, PANalytical, EMPYREAN). Graphitic structure and surface functional groups of all synthesized carbons were studied with a Raman spectroscopy and a Fourier transform infrared spectrometer (FT-IR, Bruker, TENSOR27), respectively. A contact angle meter (First Ten Angstroms FTA1000 Drop Shape Instrument B Frame Analyzer System, USA) was used to estimate the contact angle between water and the carbon surface to identify carbon wettability. X-ray photoelectron spectroscopy (XPS) analysis was employed to investigate the chemical composition of all carbons. The XPS is located at Beamline 3.2U of Synchrotron Light Research Institute (SLRI), Thailand. Specific surface areas, total specific pore volumes, and average pore sizes of the synthesized products were measured by N_2 adsorption/desorption and a BET method (High Throughput Surface Area and Porosity Analyzer, Micromeritics, ASAP2460).

2.4 Electrochemical characterization

The synthesized products were electrochemically characterized via cyclic voltammetry (CV), galvanostatic charge/discharge (GCD), and electrochemical impedance spectroscopy (EIS) (Wuhan Corrtest Instruments Corp. Ltd., China) on a three-electrode mode. The carbon electrode, Ag/AgCl, and platinum (Pt) plate were employed as a working electrode, reference electrode, and counter electrode, respectively, in 6 M KOH aqueous electrolyte. The CV measurement was tested at varying scan rates of 10, 20, 30, 40, 50, and 100 mV s^{-1} . The GCD tests were taken at varying current densities of 0.5, 1, 2, 3, 4, and 5 A g^{-1} . The EIS data were tested at a 5 mV AC amplitude in a frequency range from 100 kHz to

0.01 Hz. Specific capacitances (C) of the carbon electrodes were calculated based on Eqs. (1) and (2)

$$C = \frac{\int IdV}{2mv\Delta V} \text{ (For CV)}, \quad (1)$$

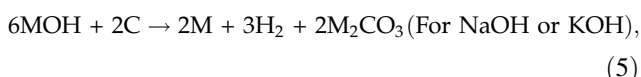
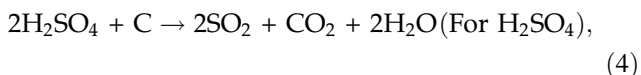
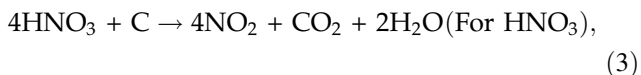
$$C = \frac{I\Delta t}{m\Delta V} \text{ (For GCD)}, \quad (2)$$

where $\int IdV$, m , v , ΔV , I , and Δt denote the integrated area of a CV curve, mass of the active material on the Ni foam, scan rate, potential range (1.2 V), constant discharge current, and discharging time, respectively.

3 Results and discussion

3.1 Structural characterization

Morphologies of the synthesized carbons are shown in Fig. 1. The non-AC in Fig. 1a has a smooth and dense surface. In contrast, the morphologies of the AC-HNO₃, AC-H₂SO₄, AC-NaOH, and AC-KOH samples, in Fig. 1b–e, show a great number of macropores owing to etching by the chemical agents (HNO₃, H₂SO₄, NaOH, and KOH) during the chemical activation process. The etching process removed some of the carbon atoms from the carbon substance, and their etching reactions are as follows [30–33]:



where M is the metal Na or K. After the chemical reaction, some carbons are turned into CO₂ by an acidic agent (HNO₃ or H₂SO₄) [30, 31], or become Na₂CO₃ or K₂CO₃ when basic NaOH or KOH is added [32, 33], respectively. This leads to the formation of micropores or mesopores on the activated carbons as seen in Fig. 1b–e.

EDX spectra of the synthesized carbons are presented in Fig. S1 and the elemental data are listed in Table 1. The non-AC sample contains carbon (C), oxygen (O), silicon (Si), sulfur (S), chlorine (Cl), and copper (Cu). The carbon, oxygen, silicon, and sulfur elements might originate from the components of sugarcane bagasse, while chlorine and copper from the washing process with HCl and the copper tape

used to stick the electrode powder onto the scanning electron microscopy (SEM) stub, respectively. The four AC samples are composed of elements similar to the non-AC sample. All AC powders show a lower C atomic percentage than the non-AC. This should be associated with the new functional groups formed on the samples as shown in Eqs. (3–5). A large amount of sulfur is detected on the AC-H₂SO₄ powder owing to the presence of sulfur in sugarcane bagasse and the H₂SO₄ agent. The AC-NaOH shows an additional Na element, likely as a result of the NaOH agent used in the activation process. Note that the oxygen content in the carbons activated by acid (AC-HNO₃ and AC-H₂SO₄) is lower than that of the non-AC powder, whereas the oxygen content of the carbons activated by bases (AC-NaOH and AC-KOH) is higher. As illustrated in Eqs. (3) and (4), acidic agents react with carbon resulting in the formation of CO₂. On the contrary, basic agents react with carbon to form Na₂CO₃ or K₂CO₃ (as expressed in Eq. (5)) leading to the elevation of the residue oxygen content.

XRD patterns of the five carbons as shown in Fig. 2a comprise two broad peaks at 22.85° and 43.93° indicating the presence of amorphous carbon [6, 8]. Weaker and broader peaks are found on the activated carbons compared to the peaks of the non-AC implying higher amorphous degree in the activated carbons. Raman spectra in Fig. 2b display two main peaks at 1353 and 1583 cm⁻¹, which correspond to a D and G band, respectively. The D peak is associated with the disordered structures and/or structural defects on the carbonaceous materials, whereas the graphitized carbonaceous structures are represented by the G peak [7]. The integrated intensity ratio of the D to G band (I_D/I_G) is used to determine the graphitized degree. The I_D/I_G values of the non-AC, AC-HNO₃, AC-H₂SO₄, AC-NaOH, and AC-KOH powders are 2.52, 2.39, 2.47, 2.27, and 2.20, respectively. We can see that the I_D/I_G value slightly decreases after chemical activation suggesting that the chemical activation contributes to the increase in the graphitized degree of all four ACs. The reduction in the I_D/I_G value after chemical activation has also been observed by other research groups [34–36].

Surface wettability of the synthesized carbons was estimated by the contact angle measurement, and the contact angle values are listed in Table 1. Contact angle of the non-AC is about 119.95°, which is close to the contact angle of the commercial AC (112.5°) as reported by Yan et al. [37]. The AC-NaOH and AC-

Fig. 1 SEM micrographs of **a** non-AC, **b** AC-HNO₃, **c** AC-H₂SO₄, **d** AC-NaOH, and **e** AC-KOH powders

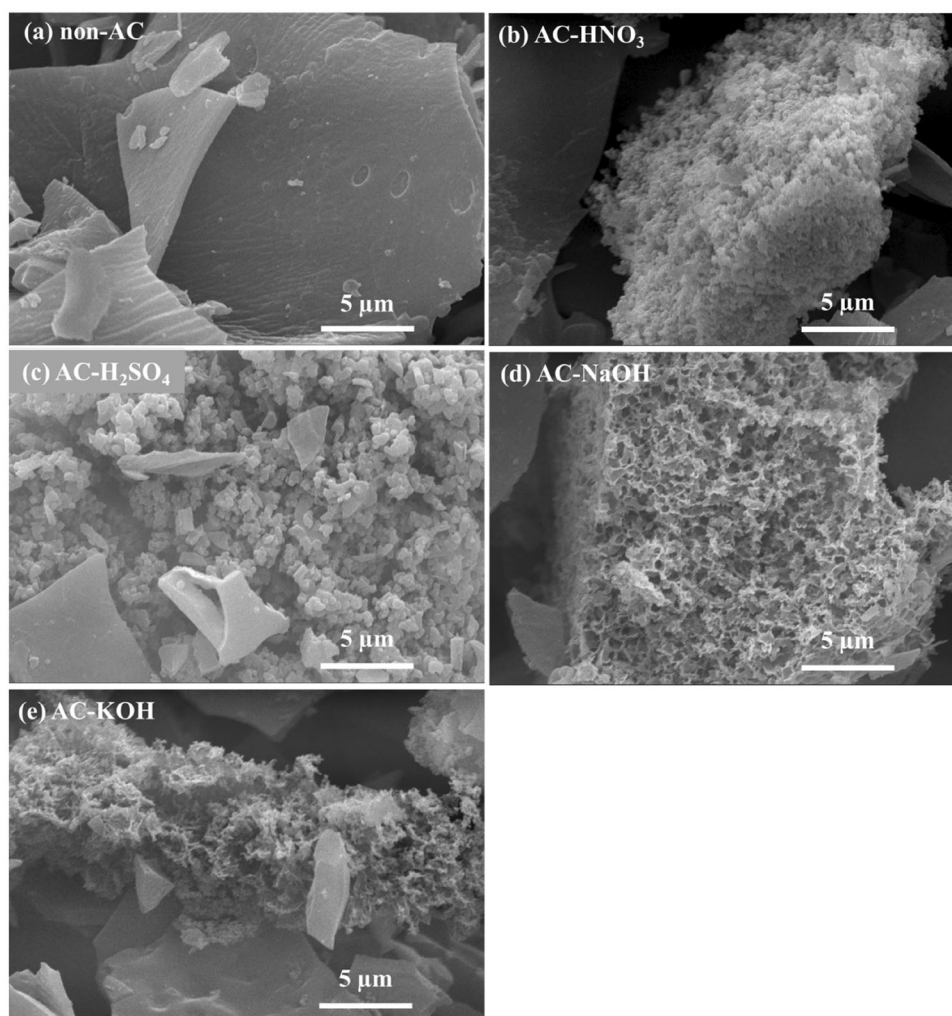


Table 1 Percentages of each element obtained from EDX and XPS data, and contact angles of all synthesized carbons

Samples	Atomic element (%)												Contact angle (deg.)
	EDX								XPS				
	C	O	Si	S	Na	Cl	Cu	Total	C 1s	O 1s	S 2p	Total	
Non-AC	91.90	6.97	0.62	0.10	–	0.14	0.27	100.00	86.87	13.13	–	100.00	119.95
AC-HNO ₃	91.03	6.06	2.09	0.05	–	0.42	0.35	100.00	83.39	16.61	–	100.00	129.02
AC-H ₂ SO ₄	90.04	5.90	1.02	2.39	–	0.21	0.44	100.00	81.75	17.99	0.26	100.00	132.24
AC-NaOH	90.70	7.43	0.29	0.22	1.00	0.08	0.27	100.00	80.16	19.84	–	100.00	99.56
AC-KOH	90.99	7.88	0.57	0.19	–	0.06	0.31	100.00	73.91	26.09	–	100.00	113.90

KOH electrodes exhibit lower contact angles, whereas the carbons modified by the acidic agents are found to have increased contact angles. The different behavior as a result of treatment either with the acidic or basic agents may be due to the differing

oxygen content present on their surfaces as shown in Table 1. It was reported by Fan et al. that a higher oxygen content resulted in a lower contact angle [38]. Thus, high surface wettability observed in the AC-

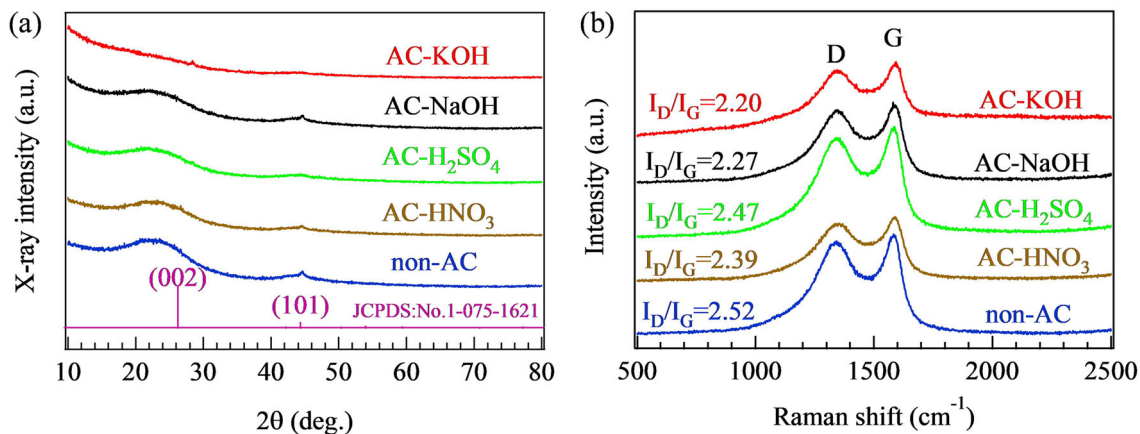


Fig. 2 a XRD and b Raman results of the non-AC, AC-HNO₃, AC-H₂SO₄, AC-NaOH, and AC-KOH

NaOH and AC-KOH electrodes are likely associated with their large oxygen contents.

Surface chemistry of the non-AC and ACs was thoroughly investigated by XPS. Figure 3 and Fig. S2 display high-resolution XPS spectra of all five carbon

powders. The high-resolution C 1s spectra in Fig. 3a show three sub-peaks at about 284.8, 287.2, and 290.0 eV ascribed to the C–C (aromatic groups), C–O (ether groups), and C=O (carbonyl groups) bonds, respectively [39–42]. The high enclosed area of the C–

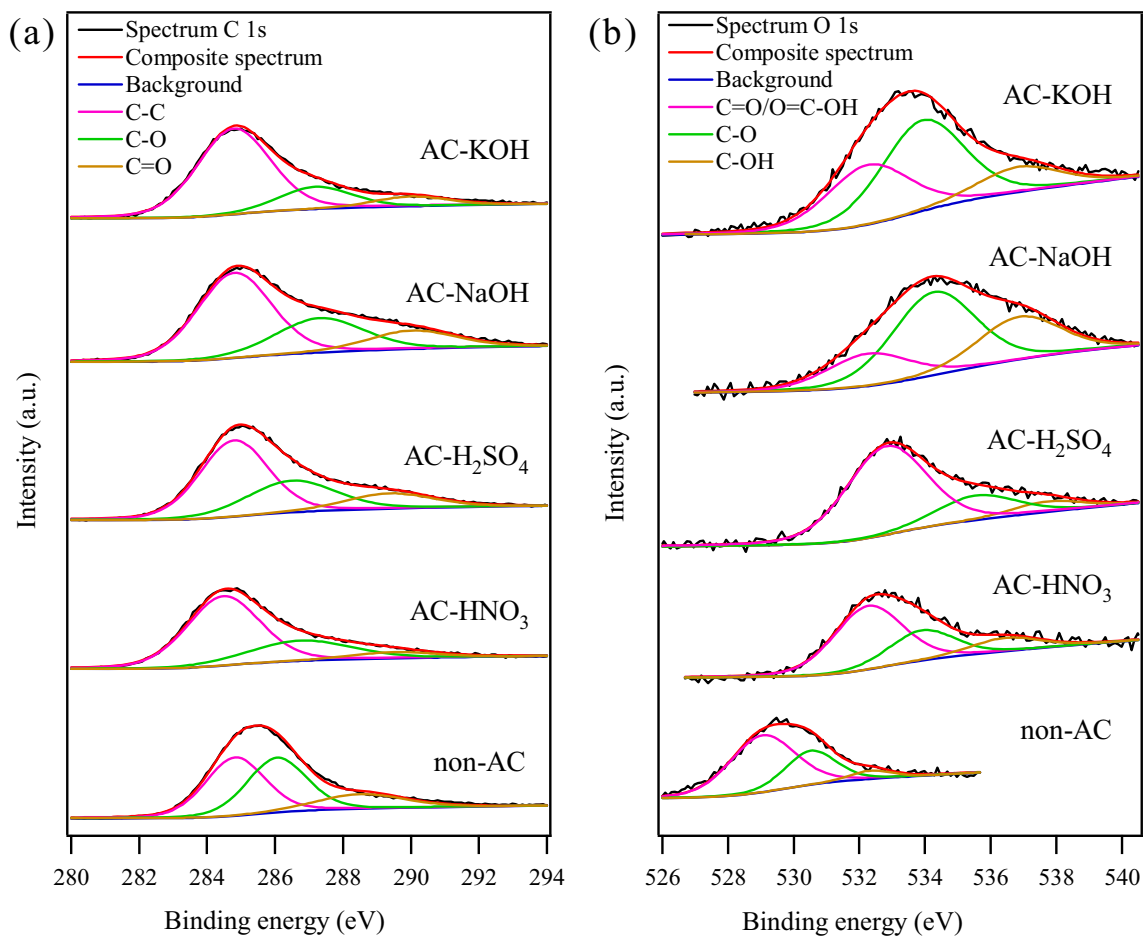


Fig. 3 a C 1s and b O 1s high-resolution XPS spectra of the non-AC, AC-HNO₃, AC-H₂SO₄, AC-NaOH, and AC-KOH powders

C and C–O sub-peaks is observed for all five samples in Fig. 3a. Deconvolution of the high-resolution O 1s spectra in Fig. 3b produces three sub-peaks at about 532.3, 533.9, and 536.9 eV corresponding to the presence of the C=O/O=C–OH (carbonyl or carboxylic groups), C–O (ether groups), and C–OH (hydroxyl groups) bonds, respectively [43]. As seen in Fig. 3b, the AC-KOH and AC-NaOH powders have a high enclosed area of the C–O sub-peak. The atomic percentages of carbon, oxygen, and/or sulfur on each sample as measured by XPS are shown in Table 1. The AC-NaOH and AC-KOH powders have higher oxygen percentages than the other three synthesized carbons. High oxygen percentages indicate the strong presence of oxygen functional groups formed as a result of treatment with the basic agents, which explain the good wettability of the AC-NaOH and AC-KOH powders.

Qualitative information on functional groups of the carbon powders were further confirmed by a FT-IR spectrometer as illustrated in Fig. 4a. All samples

exhibit similar features. The band at 1580 cm^{-1} corresponds to C–C vibrations of the aromatic ring, while the peak at 1105 cm^{-1} is related to the C–O stretching in aryl ethers [1, 7, 44]. The AC-NaOH and AC-KOH powders display relatively high C–O peak intensity implying their good hydrophilic nature [44]. The FT-IR results agree well with the XPS spectra.

Specific surface area and pore size of the non-AC and AC powders were evaluated by a N_2 adsorption/desorption measurement as displayed in Fig. 4b. The isotherm curves match a typical TYPE I. TYPE I isotherm on the activated carbons was also reported by other research groups [1, 10, 45]. Micropore and mesopore structures can be observed on all five samples as seen in Fig. 4c. The non-AC, AC- HNO_3 , and AC- H_2SO_4 samples have a pore width of 1.0–2.2 nm, whereas it is 1.1–4.0 nm for the AC-NaOH and AC-KOH (Fig. 4c). The specific surface areas, total specific pore volumes, and average pore sizes of all synthesized carbon materials are detailed in Table 2. The specific surface areas of the AC-

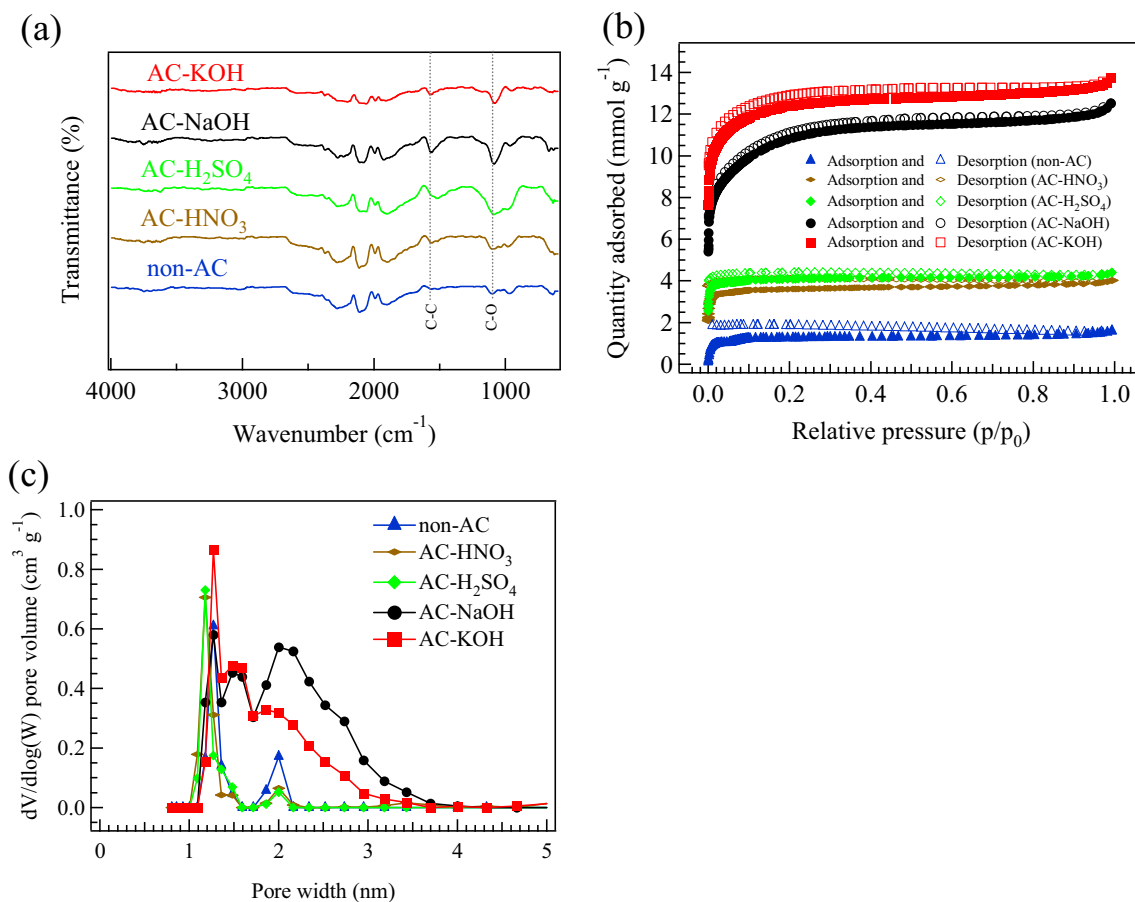


Fig. 4 a FT-IR results, b N_2 adsorption/desorption isotherms, and c distribution of pore sizes of all carbons

Table 2 Summary of specific BET surface areas, total specific pore volumes, average pore sizes, and specific capacitances from CV and GCD at respective scan rate of 10 mV s^{-1} and current density of 0.5 A g^{-1} of all carbons

Samples	Specific BET surface areas ($\text{m}^2 \text{ g}^{-1}$)	Total specific pore volumes ($\text{cm}^3 \text{ g}^{-1}$)	Average pore sizes (nm)	Specific capacitance (F g^{-1}) at 10 mV s^{-1} from CV	Specific capacitance (F g^{-1}) at 0.5 A g^{-1} from GCD
Non-AC	100.97	0.054	2.146	16.64	32.58
AC-HNO ₃	318.17	0.138	1.740	36.95	50.25
AC-H ₂ SO ₄	369.52	0.151	1.637	43.78	69.59
AC-NaOH	889.71	0.432	1.943	77.77	109.99
AC-KOH	1058.53	0.474	1.790	105.96	138.61

HNO₃, AC-H₂SO₄, AC-NaOH, and AC-KOH specimens increase to 318.17, 369.52, 889.71, and 1058.53 $\text{m}^2 \text{ g}^{-1}$, respectively, and the total specific pore volumes increase to 0.138, 0.151, 0.432, and 0.474 $\text{cm}^3 \text{ g}^{-1}$, respectively, in comparison to the specific surface area of $100.97 \text{ m}^2 \text{ g}^{-1}$ and the total specific pore volume of $0.054 \text{ cm}^3 \text{ g}^{-1}$ as obtained from the non-AC powder. In our study, the AC-KOH powder shows the largest specific surface area ($1058.53 \text{ m}^2 \text{ g}^{-1}$) and the highest total specific pore volume ($0.474 \text{ cm}^3 \text{ g}^{-1}$), which is higher than those of the AC derived from coffee shells undergoing ZnCl₂ treatment ($842 \text{ m}^2 \text{ g}^{-1}$ and $0.467 \text{ cm}^3 \text{ g}^{-1}$) in Jisha et al.'s work [46].

3.2 Electrochemical characterization

Figure 5a displays the CV curves of all carbon electrodes at the scan rate of 10 mV s^{-1} in the potential window from -1.2 to 0 V . The curves show a rectangular profile for all electrodes, implying a nearly ideal EDLC behavior [1, 2, 6]. Specific capacitances from the CV curves of all carbon electrodes at 10 mV s^{-1} , calculated by Eq. (1), are listed in Table 2. Specific capacitances of the AC electrodes is higher than that of the non-AC (16.64 F g^{-1}). Particularly, the AC-KOH electrode produces the highest specific capacitance of 105.96 F g^{-1} , likely attributed to the highest specific surface area, smallest average pore size, highest total specific pore volume (Table 2), and best wettability (Table 1) of the AC-KOH powder. Hu et al. [44] also reported that activated carbon fiber (ACF) treated with KOH (KOH-ACF) had a higher specific capacitance (344 F g^{-1} at 10 mV s^{-1}) than the activated carbon fiber treated with NaOH (NaOH-ACF) ($\sim 150 \text{ F g}^{-1}$ at 10 mV s^{-1}) and pure carbon fiber (CF) ($\sim 75 \text{ F g}^{-1}$ at 10 mV s^{-1}). The KOH-ACF electrode had a smaller pore size and a larger

graphite basal plane size than those of the NaOH-ACF and non-activated carbon fiber electrodes.

The rectangular CV curve of the AC-KOH electrode (Fig. 5b) can be preserved at the high scan rate of 100 mV s^{-1} , which implies the excellent rate capability. Figure 5c shows the calculated specific capacitances of all electrodes from various CV scan rates. The AC-KOH electrode produces the highest specific capacitance for every scan rate. The specific capacitances of all five electrodes show a decreasing trend with increasing scan rate (Fig. 5c). This is owed to the short ion movement time at high scan rates, which induces most ion accommodation on the exterior electrode [9].

The galvanostatic charge/discharge (GCD) of the first cycle of the five carbon electrodes at the current density of 0.5 A g^{-1} is illustrated in Fig. 6a. All electrodes exhibit a nearly triangular shape indicating the ideal EDLC behavior [17]. The specific capacitances of the non-AC, AC-HNO₃, AC-H₂SO₄, AC-NaOH, and AC-KOH electrodes evaluated by Eq. (2) are 32.58, 50.25, 69.59, 109.99, and 138.61 F g^{-1} , respectively, as summarized in Table 2. The GCD curves of the carbon electrodes in Fig. 6b and Fig. S3 show a reduction in the discharge time with an increase in current density. As can be seen in Fig. 6c, the AC-KOH electrode delivers the highest specific capacitance of 138.61 F g^{-1} at the current density of 0.5 A g^{-1} and the best rate capability retention of 68.98% of its initial specific capacitance after the current density of 5 A g^{-1} .

To explain the electrochemical characteristic of these electrodes, EIS measurement was performed. Nyquist plots in Fig. 6d were fitted using an equivalent circuit model as shown in Fig. 6e. R_s and R_{ct} refer to the series resistance and the charge transfer resistance at the interface between the electrode and the electrolyte, respectively. CPE represents the

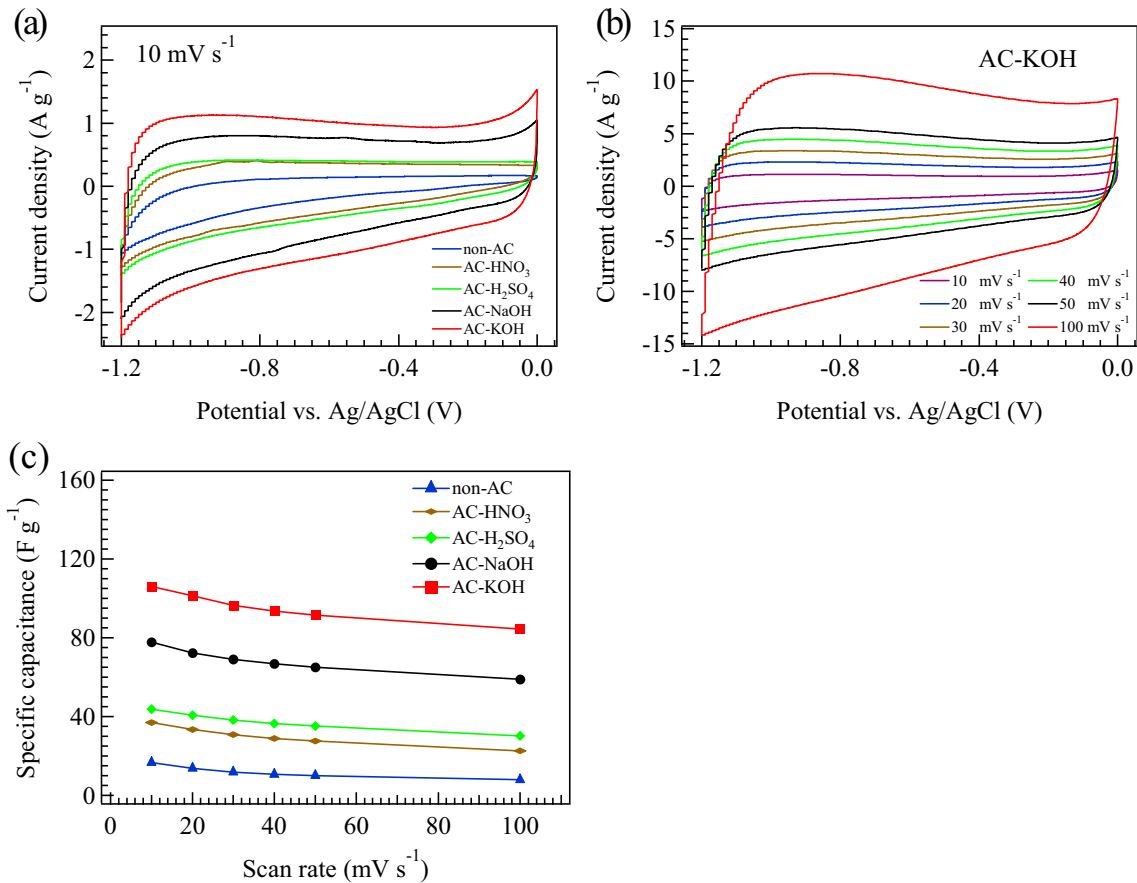


Fig. 5 **a** CV curves of the five electrodes at the scan rate of 10 mV s^{-1} , **b** CV curves of the AC-KOH electrode at various scan rates from 10 to 100 mV s^{-1} , and **c** specific capacitances of all carbon electrodes at different scan rates from 10 to 100 mV s^{-1}

constant phase element, which can be divided into a capacitive value ($CPE-T$) and a constant phase element exponent ($CPE-P$) [47, 48]. W refers to the Warburg impedance of an ionic diffusion in the electrolyte, composed of a diffusion resistance ($W-R$), a diffusion time constant ($W-T$), and a Warburg exponent ($W-P$) [47–49]. The fitted values of all parameters are listed in Table 3. The fitted R_s values were measured to be 0.94, 0.93, 0.86, 0.89, and 0.86Ω for the non-AC, AC-HNO₃, AC-H₂SO₄, AC-NaOH, and AC-KOH electrodes, respectively. Moreover, the R_{ct} values are 0.35, 0.31, 0.29, 0.01, and 0.03Ω for the non-AC, AC-HNO₃, AC-H₂SO₄, AC-NaOH, and AC-KOH electrodes, respectively. The small R_{ct} values observed on the AC-NaOH and AC-KOH electrodes imply rapid transfer of charges at the electrode and the electrolyte interfaces.

This should be attributed to the good wettability and large mesopores of the AC-NaOH and AC-KOH samples as evidenced by the contact angle and the N₂ adsorption/desorption measurement, respectively.

The AC-NaOH and AC-KOH electrodes also show a small impedance value for the entire frequency from 100 kHz to 0.01 Hz as seen in Fig. 6f. This indicates that the AC-NaOH and AC-KOH electrodes have high electrical conductivity. Electrode stability was tested for 1000 GCD cycles, as shown in Fig. 7. All five carbon electrodes possess excellent specific capacitance retention of almost 100% after 1000 GCD cycles. The specific capacitance retentions of the non-AC, AC-HNO₃, and AC-H₂SO₄ electrodes slightly increase after 1000 GCD cycles. This should be due to the low electrode wettability (as evidenced from the large contact angle of 119.95° , 129.02° , and 132.24° , respectively) causing the low ion diffusion rate into the electrodes. The longer charge/discharge cycles may allow more electrolytes penetrating to the electrode, which results in the increasing specific capacitance.

Based on our results, it can be inferred that the key factors for the excellent performance of the carbon electrodes are their high specific surface area, high

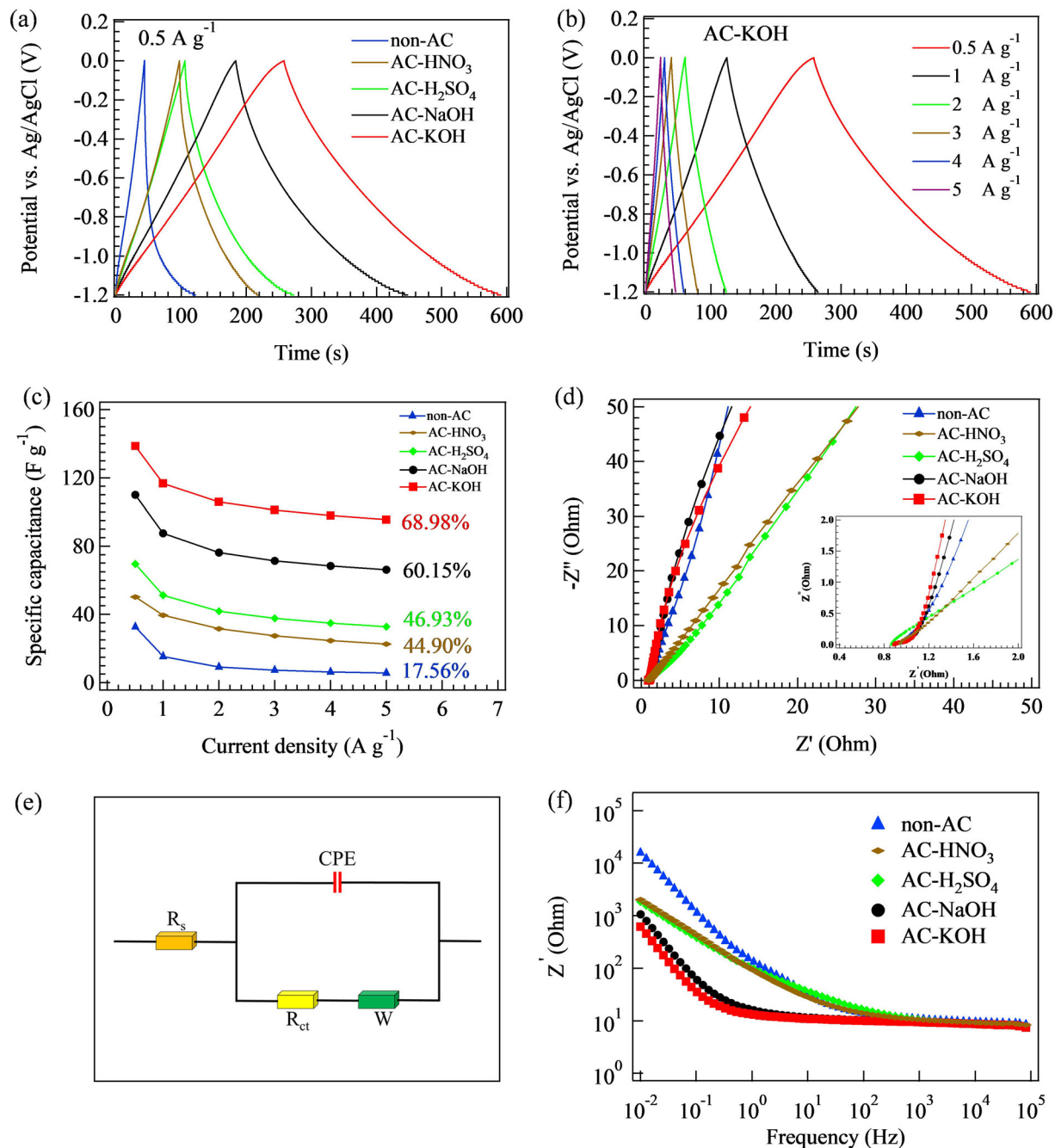


Fig. 6 **a** GCD curves of all the five carbon electrodes at the current density of 0.5 A g^{-1} , **b** GCD curves of AC-KOH electrode at various current densities from 0.5 to 5 A g^{-1} , **c** specific capacitances of all the five carbon electrodes at current densities

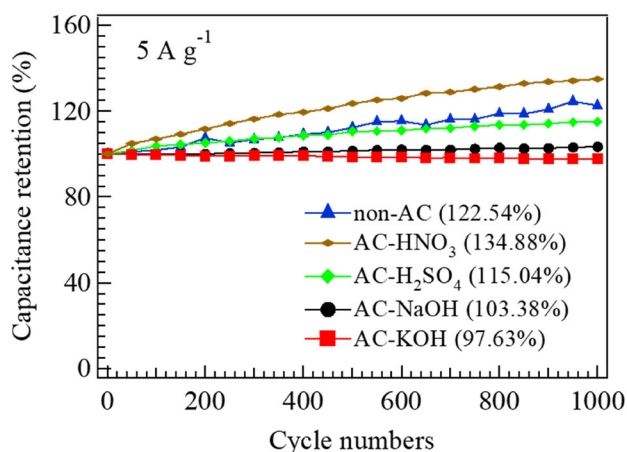
total specific pore volume, large pore width, good electrode wettability, and high electrical conductivity. The acidic agents (HNO_3 and H_2SO_4) can slightly improve the specific surface areas, the total specific pore volumes, and the electrical conductivity of the carbons, but they exhibit lower surface wettability. In

varying from 0.5 to 5 A g^{-1} , **d** Nyquist plots of all electrodes, **e** an equivalent circuit model, and **f** impedance spectra of all the five carbon electrodes plotted between frequency and z'

the case of the basic agents (NaOH and KOH), similar parameters can significantly be enhanced with an added advantage of good electrode wettability. Among the four chemical agents, the use of KOH results in the highest specific capacitance of the electrode because this basic agent not only improves

Table 3 Summary of the parameters evaluated from the fitting of EIS results of all electrodes

Electrodes	R_s (Ω)	R_{ct} (Ω)	CPE		W		
			CPE-T (mF)	CPE-P	W-R (Ω)	W-T (10^{-3} s)	W-P
Non-AC	0.94	0.35	1.97	0.83	3.00	1.93	0.48
AC-HNO ₃	0.93	0.31	10.63	0.68	3.33	3.18	0.36
AC-H ₂ SO ₄	0.86	0.29	6.81	0.69	15.32	76.48	0.36
AC-NaOH	0.89	0.01	17.16	0.67	1.48	55.30	0.52
AC-KOH	0.86	0.03	19.52	0.55	1.00	77.51	0.51

**Fig. 7** Specific capacitance retention of all five carbon electrodes at the current density of 5 A g^{-1}

all of the parameters stated above but it can also produce a great number of micropores (smaller than 2 nm) and/or mesopores (2–50 nm) on/inside the carbon structures.

4 Conclusion

Activated carbon (AC) from sugarcane bagasse was successfully used in the supercapacitor application. The synthesized AC powders have a lot of macropores with high specific surface area, high total specific pore volume, large pore width, good electrode wettability, and high electrical conductivity. The AC-KOH electrode was found to have the largest specific surface area of $1058.53 \text{ m}^2 \text{ g}^{-1}$ and the highest total specific pore volume of $0.474 \text{ cm}^3 \text{ g}^{-1}$, both of which contribute to its having the highest specific capacitance (138.61 F g^{-1}) among the studied AC electrodes. Furthermore, good rate capability (68.98%) and good electrode stability (100%) can be achieved from the AC-KOH electrode.

Acknowledgements

This work has been partially supported by the Research Network NANOTEC (RNN) program of the National Nanotechnology Center (NANOTEC), NSTDA, Ministry of Higher Education, Science, Research and Innovation and Khon Kaen University, Thailand and by National Research Council of Thailand (NRCT) (Contract No. 6200072) and Research and Academic Affairs Promotion Fund, Faculty of Science, Khon Kaen University, Fiscal year 2019 (RAAPF), by Thailand Science Research and Innovation and Srinakharinwirot University (Contract No. 028/2564). A. Phakkhawan is grateful to the Development and Promotion of Science and Technology Talents Project (DPST) for providing a scholarship.

Supplementary Information: The online version contains supplementary material available at <http://doi.org/10.1007/s10854-021-07334-y>.

References

1. M. Sivachidambaram, J.J. Vijaya, L.J. Kennedy, R. Jothiralingam, H.A. Al-Lohedan, M.A. Munusamy, E. Elanthamilan, J.P. Merlin, *New J. Chem.* **41**, 3939 (2017)
2. W. Du, Z. Zhang, L. Du, X. Fan, Z. Shen, X. Ren, Y. Zhao, C. Wei, S. Wei, *J. Alloys Compd.* **797**, 1031 (2019)
3. S. Ahmed, M. Rafat, A. Ahmed, *Adv. Nat. Sci.: Nanosci. Nanotechnol.* **9**, 035008 (2018)
4. C.S. Yang, Y.S. Jang, H.K. Jeong, *Curr. Appl. Phys.* **14**, 1616 (2014)
5. Y. Zhao, Y. Meng, P. Jiang, *J. Power Sources* **259**, 219 (2014)
6. G. Zhang, Y. Chen, Y. Chen, H. Guo, *Mater. Res. Bull.* **102**, 391 (2018)
7. F. Guo, X. Jiang, X. Jia, S. Liang, L. Qian, Z. Rao, *J. Electroanal. Chem.* **844**, 105 (2019)

8. S. Zhang, Q. Zhang, S. Zhu, H. Zhang, X. Liu, *Energy Sources A* (2019). <https://doi.org/10.1080/15567036.2019.1624881>
9. L. Zhu, F. Shen, R.L. Smith, L. Yan, L. Li, X. Qi, *Chem. Eng. J.* **316**, 770 (2017)
10. K.M. Horax, S. Bao, M. Wang, Y. Li, *Chin. Chem. Lett.* **28**, 2290 (2017)
11. A. Phakkhawan, P. Klangtakai, A. Chompoosor, S. Pimanpang, V. Amornkitbamrung, *J. Mater. Sci.: Mater. Electron.* **29**, 9406 (2018)
12. A. Kurniawan, L.K. Ong, F. Kurniawan, C.X. Lin, F.E. Soetaredjo, X.S. Zhao, S. Ismadji, *RSC Adv.* **4**, 34739 (2014)
13. Z.S. Iro, C. Subramani, S.S. Dash, *Int. J. Electrochem. Sci.* **11**, 10628 (2016)
14. R.R. Salunkhe, S.H. Hsu, K.C.W. Wu, Y. Yamauchi, *ChemSuschem* **7**, 1551 (2014)
15. P. Tagsin, P. Klangtakai, V. Harnchana, V. Amornkitbamrung, S. Pimanpang, P. Kumnorkaen, *J. Korean Phys. Soc.* **71**, 997 (2017)
16. D. Ganguly, D. Pahari, N.S. Das, P. Howli, B. Das, D. Banerjee, K.K. Chattopadhyay, *J. Electroanal. Chem.* **778**, 12 (2016)
17. C. Dai, J. Wan, J. Shao, F. Ma, *Mater. Lett.* **193**, 279 (2017)
18. M.A. Nazem, M.H. Zare, S. Shirazian, *RSC Adv.* **10**, 1463 (2020)
19. K.Z. Yan, M.A.A. Zaini, A. Arsad, N.S. Nasri, *Chem. Eng. Trans.* **72**, 151 (2019)
20. R. Taslim, T.R. Dewi, E. Taer, A. Apriwandi, A. Agustino, R.N. Setiadi, *J. Phys.: Conf. Ser.* **1120**, 012084 (2018)
21. H. Jin, J. Hu, S. Wu, X. Wang, H. Zhang, H. Xu, K. Lian, *J. Power Sources* **384**, 270 (2018)
22. E.Y.L. Teo, L. Muniandy, E.P. Ng, F. Adam, A.R. Mohamed, R. Jose, K.F. Chong, *Electrochim. Acta* **192**, 110 (2016)
23. K. Chaitra, R.T. Vinny, P. Sivaraman, N. Reddy, C. Hu, K. Venkatesh, C.S. Vivek, N. Nagaraju, N. Kathyayini, *J. Energy Chem.* **26**, 56 (2017)
24. W.L. Zhang, J.H. Xu, D.X. Hou, J. Yin, D.B. Liu, Y.P. He, H.B. Lin, *J. Colloid Interface Sci.* **530**, 338 (2018)
25. E. Taer, W.S. Mustika, F. Agustino, N. Hidayu, R. Taslim, *IOP Conf. Ser.: Earth Environ. Sci.* **58**, 012065 (2017)
26. A. Jain, S.K. Tripathi, *J. Energy Storage* **4**, 121 (2015)
27. K.L. Van, T.T.L. Thi, *Prog. Nat. Sci.: Mater. Int.* **24**, 191 (2014)
28. V. Subramanian, C. Luo, A.M. Stephan, K.S. Nahm, S. Thomas, B. Wei, *J. Phys. Chem. C* **111**, 7527 (2007)
29. M. Doloksaribu, B. Prihandoko, K. Triyana, *Int. J. Sci.: Basic Appl. Res.* **35**, 430 (2017)
30. B. Khalid, Q. Meng, R. Akram, B. Cao, *Desalin. Water Treat.* **57**, 2195 (2016)
31. M.T. Izquierdo, B. Rubio, *J. Hazard. Mater.* **155**, 199 (2008)
32. R.L. Tseng, *J. Colloid Interface Sci.* **303**, 494 (2006)
33. F.O. Ochai-Ejeh, A. Bello, J. Dangbegnon, A.A. Khaleed, M.J. Madito, F. Bazegar, N. Manyala, *J. Mater. Sci.* **52**, 10600 (2017)
34. D. Jia, X. Yu, H. Tan, X. Li, F. Han, L. Li, H. Liu, *J. Mater. Chem. A* **5**, 1516 (2017)
35. M. Baysal, K. Bilge, B. Yilmaz, M. Papila, Y. Yürüm, *J. Environ. Chem. Eng.* **6**, 1702 (2018)
36. J. Phiri, J. Dou, T. Vuorinen, P.A.C. Gane, T.C. Maloney, *ACS Omega* **4**, 18108 (2019)
37. J. Yan, H. Zhang, Z. Xie, J. Liu, *AIP Conf. Proc.* **1864**, 020218 (2017)
38. L.Z. Fan, S. Qiao, W. Song, M. Wu, X. He, X. Qu, *Electrochim. Acta* **105**, 299 (2013)
39. G. Zhou, C. Xu, W. Cheng, Q. Zhang, W. Nie, *J. Anal. Methods Chem.* **2015**, 467242 (2015)
40. A. Aldana-Pérez, L. Lartundo-Rojas, R. Gómez, M.E. Niño-Gómez, *Fuel* **100**, 128 (2012)
41. Y. Yao, Y. Guo, W. Du, X. Tong, X. Zhang, *J. Mater. Sci.: Mater. Electron.* **29**, 17695 (2018)
42. Q. Liang, L. Ye, Z.H. Huang, Q. Xu, Y. Bai, F. Kang, Q.H. Yang, *Nanoscale* **6**, 13831 (2014)
43. I.I. Gurten Inal, Z. Aktas, *Appl. Surf. Sci.* **514**, 145895 (2020)
44. S. Hu, S. Zhang, N. Pan, Y.L. Hsieh, *J. Power Sources* **270**, 106 (2014)
45. L. Zhang, H. Gu, H. Sun, F. Cao, Y. Chen, G.Z. Chen, *Carbon* **132**, 573 (2018)
46. M.R. Jisha, Y.J. Hwang, J.S. Shin, K.S. Nahm, T.P. Kumar, K. Karthikeyan, N. Dhanikaivelu, D. Kalpana, N.G. Renganathan, A.M. Stephan, *Mater. Chem. Phys.* **115**, 33 (2009)
47. M. Jana, P. Samanta, N.C. Murmu, T. Kuila, *J. Mater. Chem. A* **5**, 12863 (2017)
48. M. Jana, S. Saha, P. Khanra, P. Samanta, H. Koo, N.C. Murmu, T. Kuila, *J. Mater. Chem. A* **3**, 7323 (2015)
49. Y. Xie, H. Du, *RSC Adv.* **5**, 89689 (2015)

Publisher's Note Springer Nature remains neutral with regard to jurisdictional claims in published maps and institutional affiliations.